

Spin dephasing in n -type GaAs quantum wells in the presence of high electric fields

M. Q. Weng,^{1,2} M. W. Wu,^{1,2,*} and L. Jiang²

¹Structure Research Laboratory, University of Science and Technology of China, Academia Sinica, Hefei, Anhui, 230026, China

²Department of Physics, University of Science and Technology of China, Hefei, Anhui, 230026, China[†]

(Dated: October 26, 2019)

We perform a study of the effect of the high in-plane electric field on the spin precession and spin dephasing due to the D'yakonov-Perel' mechanism in n -type GaAs (100) quantum wells by constructing and numerically solving the kinetic Bloch equations. We include all of the scattering such as electron-phonon, electron-non-magnetic impurity as well as the electron-electron Coulomb scattering in our theory and systematically investigate how the spin precession and spin dephasing are affected by the high electric field under various conditions. The hot-electron distribution functions and the spin correlations are calculated rigorously in our theory. It is found that the D'yakonov-Perel' term in the electric field provides a non-vanishing effective magnetic field that alters the spin precession period. Moreover, spin dephasing is markedly affected by the electric field. The contribution of the electron-electron scattering to the spin dephasing is also discussed.

PACS numbers: 72.25.Rb, 72.20.Ht, 71.10.-w, 67.57.Lm, 73.61.Ey

I. INTRODUCTION

Spintronics is an active field which studies processes that manipulate the spin degree-of-freedom of electrons, with the goal of developing new electronic devices with improved performance and new functionality compared to the traditional ones which are based on precise control of the charge distribution of electrons.^{1,2} Understanding spin dephasing is an important prerequisite for the realization of such devices. As most of the semiconductor electronic devices are very small and even a small applied voltage gives a strong electric field, these devices usually work in the hot-electron condition.^{3,4} Therefore understanding spin dephasing in the presence of a strong electric field is of particular importance to the spintronic application.

Recent experiments have shown that the electron spin lifetime is very long in n -type Zinc-blende semiconductors (up to 100 ns in bulk).^{5,6,7,8,9,10,11} In theory the spin dephasing in semiconductors without high electric field has been extensively studied. Three spin dephasing mechanisms have been proposed:¹² the Elliot-Yaffet mechanism^{13,14} which is important in the narrow-bandgap and/or high impurity-doped semiconductors; the Bir-Aronov-Pikus mechanism¹⁵ which is important in the pure or p -type semiconductors; and the D'yakonov-Perel' (DP) mechanism¹⁶ which is the main spin-dephasing mechanism in n -type Zinc-blende semiconductors such as GaAs and InAs. The DP mechanism originates from the spin-orbit interaction in crystal without the inversion center and results in spin splitting of the conduction band at $k \neq 0$. This is equivalent to an effective magnetic field acting on the spin, with its magnitude and orientation depending on the electron wavevector. Moreover, an important many-body spin dephasing mechanism due to combined effects of the inhomogeneous broadening of the spin precession and the spin conserving scattering has been proposed recently^{17,18} and closely studied.^{19,20,21,22,23,24,25}

The study of the effect of electric fields on electron spins in semiconductors just begins. Experiments have shown that the spin polarization is not destroyed by the strong applied electric field in transport up to a few kV/cm.^{26,27} It is revealed that under right configurations the electric field can drive the electrons to approach a larger spin injection length.^{2,28,29,30,31,32,33,34,35,36,37} The electric manipulation of the spin of two-dimensional (2D) electrons through the Rashba^{38,39} spin-orbital interactions using the in-plane AC electric field has also been proposed.⁴⁰ Nonetheless how the hot electron effect affects the spin dephasing/transport is so far not yet studied. A complete understanding of the hot-electron effect on the spin dephasing in n -type GaAs quantum wells (QW's) can be obtained by solving the many-body kinetic Bloch equations^{17,18,19,41} which have been applied successfully to studying the spin dephasing^{22,23,24,25} and spin transport recently.^{42,43,44}

In this paper, we use the many-body kinetic equations to study the effect of the high electric field on the spin dephasing. The paper is organized as following: In Sec. II we present the model and construct the kinetic Bloch equations. Then we show the effect of the electric field on the spin dephasing problem by numerically solving the kinetic equations. In Sec. III(A) we first discuss how the electric field affects the spin precession. Then we devote ourselves to the understanding of the effect of high electric field on spin dephasing under various conditions, such as at different impurity densities; temperatures; and initial spin polarizations. We summarize the main results in Sec. IV. In Appendix A we present the effect of the electron-electron Coulomb scattering on the spin dephasing. The scheme of the numerical approach is explicated in the Appendix B.

II. MODEL AND KINETIC EQUATIONS

We start our investigation of an n -type (100) GaAs QW of width a with its growth direction along the z -axis. A uniform electric field \mathbf{E} and a moderate magnetic field \mathbf{B} are applied along the x -axis (Vogit configuration). Due to the confinement of the QW, the momentum along the z -axis of electrons is quantized. Therefore the electrons are characterized by a subband index n and a two-dimensional momentum $\mathbf{k} = (k_x, k_y)$, together with a spin index $\sigma (= \pm 1/2)$. For simplicity, we only consider the wells of a small width so that the separation of the subband energy is large enough and therefore only the lowest subband is populated and the transition to the upper subbands is unimportant. It is noted that due to the so called “runaway” effect, the single subband model is valid only when the electric field is less than a few kV/cm.^{45,46} This is because when the electric field is above the threshold value, electrons gain energy from the field faster than they can dissipate it by emitting phonons and therefore the transition to upper subbands becomes significant. Consequently in the present paper we only study the case with the electric field up to 1 kV/cm which is sufficiently large to produce the hot-electron effect.

For n -type samples, spin dephasing mainly comes from the DP mechanism.^{12,16} With the DP term included, the Hamiltonian of the electrons in the QW is given by:

$$H = \sum_{\mathbf{k}\sigma\sigma'} \left\{ (\varepsilon_{\mathbf{k}} - e\mathbf{E} \cdot \mathbf{R}) \delta_{\sigma\sigma'} + [g\mu_B \mathbf{B} + \mathbf{h}(\mathbf{k})] \cdot \frac{\boldsymbol{\sigma}_{\sigma\sigma'}}{2} \right\} c_{\mathbf{k}\sigma}^\dagger c_{\mathbf{k}\sigma'} + H_I. \quad (1)$$

Here $\varepsilon_{\mathbf{k}} = \mathbf{k}^2/2m^*$ is the energy spectrum of the electron with momentum \mathbf{k} and effective mass m^* . $\boldsymbol{\sigma}$ are the Pauli matrices. $\mathbf{R} = (x, y)$ is the position. $\mathbf{h}(\mathbf{k})$ represents the DP term which serves as an effective magnetic field with its magnitude and direction depending on \mathbf{k} . It is composed of the Dresselhaus term⁴⁷ and the Rashba term.^{38,39} For GaAs QW, the leading term is the Dresselhaus term which can be written as:

$$\begin{aligned} h_x(\mathbf{k}) &= \gamma k_x (k_y^2 - \langle k_z^2 \rangle); \\ h_y(\mathbf{k}) &= \gamma k_y (\langle k_z^2 \rangle - k_x^2); \\ h_z(\mathbf{k}) &= 0. \end{aligned} \quad (2)$$

Here $\langle k_z^2 \rangle$ represents the average of the operator $-(\frac{\partial}{\partial z})^2$ over the electronic state of the lowest subband and is therefore $(\pi/a)^2$. $\gamma = (4/3)(m^*/m_{cv})(1/\sqrt{2m^*E_g})(\eta/\sqrt{1-\eta/3})$ and $\eta = \Delta/(E_g + \Delta)$, in which E_g denotes the band gap; Δ represents the spin-orbit splitting of the valence band; and m_{cv} is a constant close in magnitude to free electron mass m_0 .⁴⁸ The Rashba term is proportional to the total electric field. For narrow band-gap semiconductors such as InAs, the Rashba term is dominant. Whereas for wide band-gap semiconductors like GaAs, it is marginal in the

regime of the applied electric field we study. The interaction Hamiltonian H_I is composed of the Coulomb interaction H_{ee} , the electron-phonon scattering H_{ph} , as well as the electron-impurity scattering H_i . Their expressions can be found in textbooks.^{49,50}

In order to study the hot-electron effect on spin dephasing, we limit our system to a spacial homogeneous one in order to avoid the additional complicity such as charge/spin diffusion. The kinetic Bloch equations in such a system are constructed using the nonequilibrium Green function method with the gradient expansion⁵⁰ and can be written as:

$$\dot{\rho}_{\mathbf{k},\sigma\sigma'} - e\mathbf{E} \cdot \nabla_{\mathbf{k}} \rho_{\mathbf{k},\sigma\sigma'} = \dot{\rho}_{\mathbf{k},\sigma\sigma'}|_{\text{coh}} + \dot{\rho}_{\mathbf{k},\sigma\sigma'}|_{\text{scatt}}, \quad (3)$$

where $\rho_{\mathbf{k}\sigma\sigma'}$ represent the single particle density matrix elements. The diagonal terms describe the electron distribution functions $\rho_{\mathbf{k},\sigma\sigma} \equiv f_{\mathbf{k}\sigma}$. The off-diagonal elements $\rho_{\mathbf{k},\frac{1}{2}-\frac{1}{2}} = \rho_{\mathbf{k},-\frac{1}{2}\frac{1}{2}}^* \equiv \rho_{\mathbf{k}}$ stand for the inter-spin-band polarizations (spin coherence).⁴¹ The second terms in the kinetic equations describe the momentum and energy input from the electric field \mathbf{E} . $\dot{\rho}_{\mathbf{k}\sigma\sigma'}|_{\text{coh}}$ on the right hand side of the equations describe the coherent spin precession around the applied magnetic field \mathbf{B} , the effective magnetic field $\mathbf{h}(\mathbf{k})$ from the DP term as well as the effective magnetic field from the electron-electron interaction in the Hartree-Fock approximation. $\dot{\rho}_{\mathbf{k}\sigma\sigma'}|_{\text{scatt}}$ denote the electron-impurity, the electron-phonons, as well as the electron-electron scattering. The expressions of these terms are given in Appendix B.

The initial conditions at $t = 0$ are taken to be $\rho_{\mathbf{k}}(0) = 0$ and electron distribution functions are chosen to be those of the steady state under the electric field but without the magnetic field and the DP term. Specifically $f_{\mathbf{k},\sigma}(0)$ is the steady solution of the kinetic equations (3) with the spin coherence $\rho_{\mathbf{k}}$, the magnetic field and the DP term set to be zero. This initial distribution functions can be approached by assuming that at time $-t_0$ there is no spin coherence $\rho_{\mathbf{k}}(-t_0) = 0$ and the electron distributions are just the Fermi distribution functions for each spin σ at the background temperature T :

$$f_{\mathbf{k}\sigma}(-t_0) = \left\{ \exp[(\varepsilon_{\mathbf{k}} - \mu_{\sigma})/T] + 1 \right\}^{-1}. \quad (4)$$

and then self-consistently solving the kinetic equations (3) with the magnetic field and the DP term turned off (therefore no spin precession and $\rho_{\mathbf{k}} \equiv 0$). By taking t_0 to be large enough one may get the steady state solution before $t = 0$. In Appendix A we present a typical electron distribution function in the steady state under the electric field. The imbalance of the the chemical potential $\mu_{1/2} \neq \mu_{-1/2}$ gives the initial spin polarization:

$$P = \frac{N_{e\ 1/2}(0) - N_{e\ -1/2}(0)}{N_{e\ 1/2}(0) + N_{e\ -1/2}(0)}, \quad (5)$$

where $N_{e\sigma}(t) = \sum_{\mathbf{k}} f_{\mathbf{k},\sigma}(t)$ is the number of the electrons with spin σ at time t .

III. NUMERICAL RESULTS

As one notices, all the unknowns to be solved appear in the coherent and the scattering terms nonlinearly. Therefore the kinetic Bloch equations have to be solved self-consistently to obtain the electron distribution and the spin coherence.

We numerically solve the kinetic Bloch equations in such a self-consistent fashion to obtain the temporal evolution of the electron distribution functions $f_{\mathbf{k}\sigma}(t)$ and the spin coherence $\rho_{\mathbf{k}}(t)$. Once these quantities are obtained, we are able to deduce all the quantities such as electron mobility μ and hot-electron temperature T_e for small spin polarization P as well as the spin dephasing rate for any spin polarization P . The mobility is given by $\mu = \sum_{\mathbf{k}\sigma} f_{\mathbf{k}\sigma}(0) \mathbf{k}/N_e$; the electron temperature is obtained by fitting the Boltzmann tail of the electron distribution function; whereas the spin dephasing rate is determined by the slope of the envelope of the incoherently summed spin coherence $\rho(t) = \sum_{\mathbf{k}} |\rho_{\mathbf{k}}(t)|$.^{18,41,51}

κ_{∞}	10.8	κ_0	12.9
ω_0	35.4 meV	m^*	0.067 m_0
Δ	0.341 eV	E_g	1.55 eV
g	0.44		

TABLE I: Material parameters used in the numerical calculations

We include the electron-electron, the electron-phonon and the electron-impurity scattering throughout our computation. For electron-phonon scattering, as we concentrate on the relatively high temperature regime, only electron-longitudinal optical (LO) phonon scattering is important. The numerical scheme of the solution of the kinetic equations is laid out in detail in Appendix B. The total electron density N_e , the width of the QW a and the applied magnetic field are taken to be $4 \times 10^{11} \text{ cm}^{-2}$, 15 nm and 4 T respectively. The material parameters of GaAs are listed in Table I. The numerical results are presented in Figs. 1 to 5.

A. Electric field dependence of the spin precession frequency

In Fig. 1 we plot a typical temporal evolution of the electron densities of spin up and down for a GaAs QW with initial spin polarization $P = 2.5\%$ under two electric fields $E = 0.5 \text{ kV/cm}$ and $E = -0.5 \text{ kV/cm}$ at $T = 120 \text{ K}$. $B = 4 \text{ T}$ for both cases. The corresponding incoherently summed spin coherence is also plotted in the figure. One can see from the figure that, the temporal evolutions of the electron densities and the spin coherence are similar to those in the absence of the applied electric field.^{22,23} The electron densities and the spin coherence oscillate as electron spins undergo the Larmor precession around the total (effective) magnetic field. Due to the

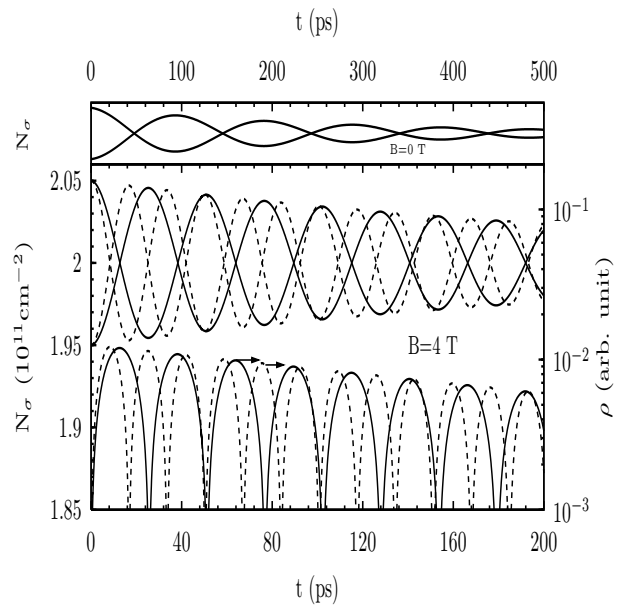


FIG. 1: Electron densities of spin up and down and the incoherently summed spin coherence ρ versus time t for a GaAs QW with initial spin polarization $P = 2.5\%$ under different electric fields $E = 0.5 \text{ kV/cm}$ (solid) and $E = -0.5 \text{ kV/cm}$ (dashed). Top panel: $B = 0 \text{ T}$; Bottom panel: $B = 4 \text{ T}$. Note the scale of the spin coherence is on the right side of the figure and the scale of the top panel is different from that of the bottom one.

spin dephasing, the amplitude of the oscillation decays exponentially. An interesting effect of the high in-plane electric field on the spin precession is that there is marked difference in the precession frequency under different electric fields (even the electric fields of the same magnitude but in the opposite directions). As shown in Fig. 1, although there is almost no difference in the corresponding spin dephasing rates, the periods of the oscillations are 51.2 ps and 33.6 ps for applied electric field $E = -0.5 \text{ kV/cm}$ and 0.5 kV/cm respectively. Both periods deviate from 40.6 ps, which is the electric-field-free one of the Larmor precession under the magnetic field $B = 4 \text{ T}$.

Moreover, it is expected that *at very low* temperature (*i.e.*, a few Kelvin) where the momentum collision rate is small, the DP term can result in a rapidly damped oscillations in the spin signal when $B = 0$. At higher temperatures, due to the higher collision rates these oscillations disappear totally and the spin polarization decays exponentially with time⁵² and the oscillations can only be seen when there is an applied magnetic field in Vogit configuration. Nevertheless, it is of particular interest to note in the top panel of Fig. 1 that even at temperature as high as 120 K, the spin signal oscillates with period 219.9 ps when there is *no* applied magnetic field but an applied electric field $E = 0.5 \text{ kV/cm}$.

Both features above originate from the applied high electric field \mathbf{E} along the x -axis. With the applied electric field, the electrons get a net center-of-mass drift velocity

V_d and the distribution function is no longer first-order-momentum free, *i.e.*, $\sum_{\mathbf{k}} \mathbf{k} f_{\mathbf{k}\sigma} = m^* V_d \neq 0$. From Eq. (2) one finds that there is a net effective magnetic field B^* along x -axis from the DP term which does not exist when $E = 0$. From the period of the spin oscillation in Fig. 1, one can deduce the effective magnetic field B^* . When electric field $E = \pm 0.5$ kV/cm, the net effective magnetic field $B^* = \mp 0.74$ T.

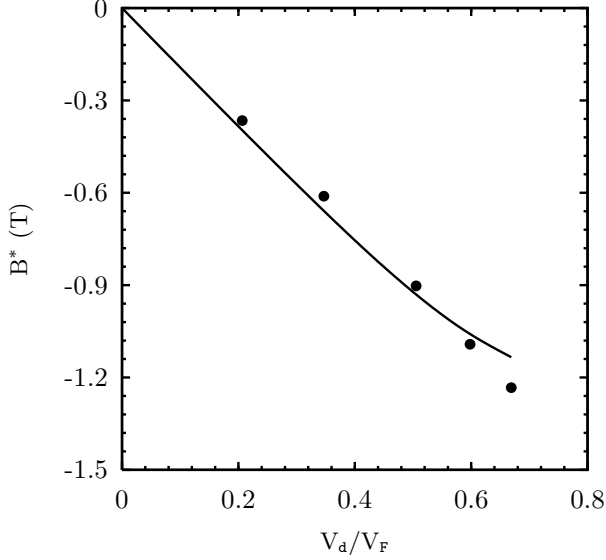


FIG. 2: The net effective magnetic field B^* from the DP term versus the drift velocity V_d at $T = 120$ K with impurity density $N_i = 0$. The solid curve is the corresponding result from Eq. (7).

The average of the total effective magnetic field the electrons experience at low spin polarization can be given approximately by:

$$\mathbf{B}_{\text{tot}} = \mathbf{B} + \mathbf{B}^* = \mathbf{B} + \frac{1}{g\mu_B} \frac{\int d\mathbf{k} (f_{\mathbf{k}1/2} - f_{\mathbf{k}-1/2}) \mathbf{h}(\mathbf{k})}{\int d\mathbf{k} (f_{\mathbf{k}1/2} - f_{\mathbf{k}-1/2})}. \quad (6)$$

By taking the electron distribution function to be the drifted Fermi function $f_{\mathbf{k}\sigma} = \{\exp[(\mathbf{k} - m^* \mathbf{V}_d)^2 / (2m^*) - \mu_\sigma] / (k_B T_e)\} + 1\}^{-1}$, the effective magnetic field for small spin polarization can be roughly estimated as following:

$$B^* = \gamma m^* {}^3 V_d \{E_f / [2(1 - e^{-E_f/k_B T_e})] - E_c\} / g\mu_B, \quad (7)$$

with E_f and E_c standing for the Fermi energy and confinement energy of the QW respectively. In Fig. 2 the effective magnetic field B^* deduced from the frequencies of our numerical result is plotted as a function of the drift velocity V_d for the impurity free sample. The result predicated by Eq. (7) is also plotted in the same figure for comparison, with the hot-electron temperature T_e obtained by fitting the Boltzmann tail of the calculated electron distribution functions. It is seen from the figure that Eq. (7) gives a reasonable estimation of B^* .

B. Electric field dependence of the spin dephasing time of electrons with small spin polarization

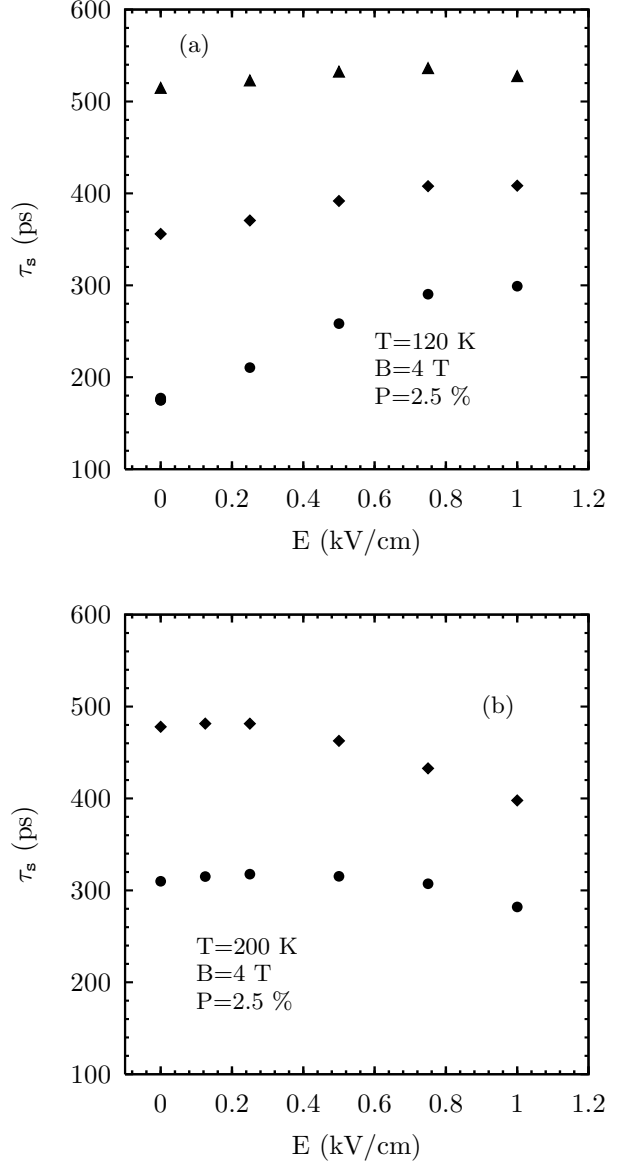


FIG. 3: The SDT τ_s versus the applied electric field E at (a) $T = 120$ K and (b) $T = 200$ K for initial spin polarization $P = 2.5\%$ with different impurity densities: \bullet , $N_i = 0$; \blacklozenge , $N_i = 0.1 N_e$; and \blacktriangle , $N_i = 0.2 N_e$.

In addition to affecting the spin precession frequency, the applied high electric field also changes the spin dephasing time (SDT), *i.e.* the inverse of the spin dephasing rate, although the electric field does not couple to the electron spin directly. In Fig. 3(a) and (b), we plot the SDT of the electrons with initial spin polarization $P = 2.5\%$ as a function of the electric field E for different impurity densities N_i at $T = 120$ K and $T = 200$ K respectively. It is seen from Fig. 3(a) that for the impurity-free sample, the SDT first increases with the

electric field from $\tau_s = 175$ ps at $E = 0$ and then saturates to $\tau_s = 300$ ps, 70 % higher when E approaches to 1 kV/cm. For samples with impurities, the SDT also increases with the electric field but with decreased increase rates for higher impurity densities. When the impurity density rises to $0.2 N_e$, τ_s first increases for small electric field and then decreases when the electric field is higher than 0.75 kV/cm. Moreover the change of the SDT with the electric field is much smaller than that of the impurity-free sample. The electric field dependence of the SDT varies as the background temperature changes. When the temperature is raised to a relatively high one, say $T = 200$ K in Fig. 3(b), the SDT increases slightly with the electric field and then decreases when $E > 0.25$ kV/cm even for the impurity-free sample.

The electric field dependence of the SDT is understood due to the concurrent effects of the high electric field and the DP term. The most obvious effect of the electric field is that the electrons get a center-of-mass drift velocity and the center of the distribution functions drift away from $\mathbf{k} = 0$. One consequence of the drift is that the DP term gives a net effective magnetic field as discussed above. This field is moderate and hence has little effect on the SDT. Another one is that because more electrons are distributed at large momentum region, the contribution from the DP term with large momentum is enhanced and the SDT can be reduced. Nevertheless, in addition to the drift, the high electric field also has another counter effect: As the high electric field gives the hot-electron effect with the electron temperature T_e higher than T , the scattering is strengthened. This can enhance the SDT.^{12,22,23} In short, the drift of the center-of-mass in the momentum space tends to reduce the SDT while the hot-electron effect helps to enhance it in the regime of our study. With these two effects considered, the electric field dependence of the SDT can be understood.

When the electric field is small, its effect on the DP term due to the drift is marginal. Therefore the SDT increases with the electric field due to the hot-electron effect when the temperature T is relatively low. As the electric field increases, the effect of the drift becomes important and the SDT saturates consequently. It is noted that the hot-electron effect is more pronounced for the system with smaller impurity density under a given electric field.⁵³ As a result, the SDT increases slower with the electric field when the impurity density is higher. For high impurity-doped samples, the hot-electron effect is markedly smaller than that of the pure ones, therefore the SDT only increases slightly in the low electric field region and then decreases as the effect of the drift dominates. Moreover, when the lattice temperature T increases, the hot-electron effect is also reduced. Therefore, in high temperature regime the drift effect becomes important even for low electric fields and it becomes possible that the SDT may drop with the increase of the electric field even for the impurity-free QW's. Moreover, the change in τ_s - E curve at high temperatures is smaller than that at low temperatures as shown in Fig. 3.

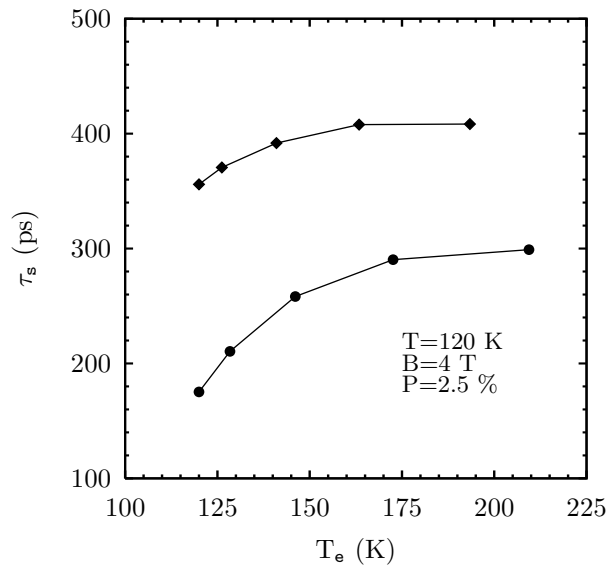


FIG. 4: SDT τ_s versus the electron temperature T_e at lattice temperature $T = 120$ K with initial spin polarization $P = 2.5$ % for $N_i = 0$ (●) and $N_i = 0.1 N_e$ (◆). The curves are plotted for the aid of the eyes.

In order to further elucidate the effect of the high electric field to the SDT, we replot the the SDT as a function of the electron temperature T_e with $T = 120$ K for $N_i = 0$ and $N_i = 0.1 N_e$ in Fig. 4. It is seen that the SDT increases with the the electron temperature T_e , similar to the electric-field-free case where the SDT increases with the temperature.^{23,24,54} The figure also shows that the impurities reduce the hot-electron effect and increase the SDT. These results indicate that for the electric fields we study, the electric field dependence of the SDT is affected mainly by the hot-electron effect in stead of the drift effect.

C. Electric field dependence of the spin dephasing time of electrons with high spin polarization

We now turn to study the effect of the electric field on the spin dephasing with high initial spin polarization. Similar problem *in the absence* of electric fields has been studied in our previous work.^{22,23,24}

The numerical results are presented in Fig. 5 where the SDT is plotted as a function of the initial spin polarization under different electric fields. It is seen from the figure that for all the electric fields we study, the SDT increases with the spin polarization as the case of $E = 0$.^{22,23,24} However the speed drops with the increase of the electric field. It is interesting to see that the electric field dependence of the SDT is quite different for different initial spin polarizations. In low polarization regime, the SDT increases with the electric field while in high polarization one, it decreases with the electric field. For moderate spin polarized electrons, the SDT is insensitive

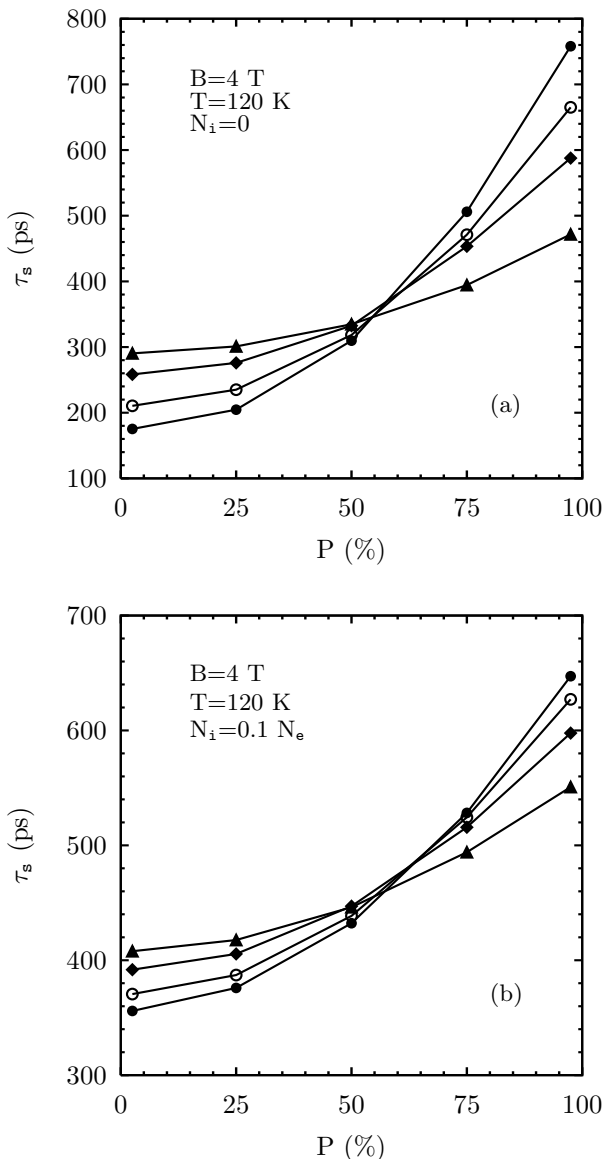


FIG. 5: The spin dephasing time τ_s (●) vs. the initial spin polarization for $T = 120$ K and $N_i = 0$ (a) and $N_i = 0.1 N_e$ (b) under different electric field: ●, $E = 0$; ○, $E = 0.25$ Kv/cm; ◆, $E = 0.5$ Kv/cm; ▲, $E = 0.75$ Kv/cm.

to the electric field.

The rise of the SDT with the initial spin polarization is understood due to the effective magnetic field from the HF term. As one component of this effective field is along the z -axis, it removes the “detuning” of the spin flip between the spin-up and -down bands and consequently suppresses the spin precession around the magnetic field and greatly reduces the spin dephasing.²² Therefore, all the factors, such as magnetic field, temperature, impurity, electron density, and applied electric field which can change the HF term, affect the spin dephasing in the high spin polarization case dramatically. These factors except the one of the electric field have been discussed

in detail in our previous work.^{22,23,24} As for the factor of the applied high electric field, both the drift and the hot-electron effects affect the HF term. The drift of the center of the mass in momentum space provides two competing effects on the HF term: One is to enhance the HF term through the net effective magnetic field B^* discussed above. The other is to destroy the HF term by increasing the DP effect. Meanwhile the hot-electron effect tends to soften the HF term through the increase of the electron temperature and the scattering rate. Our results indicate that the electric field tends to reduce the effective magnetic field from the HF term in high spin polarization regime and consequently reduce the SDT.

IV. CONCLUSION

In conclusion, we have performed a systematic investigation of the spin dephasing due to the DP mechanism in the present of high electric fields by constructing a set of kinetic Bloch equations for n -type semiconductor QW's based on the non-equilibrium Green function method with gradient expansion. In our theory, we include the in-plane electric field, the magnetic field in the Vogit configuration, the DP spin-orbital coupling and all the spin conserving scattering such as electron-phonon, electron-non-magnetic impurity as well as the electron-electron scattering. By numerically solving the kinetic equations, we study the evolution of electron distribution functions and the spin coherence of spin polarized electrons. The SDT is calculated from the slope of the incoherently summed spin coherence. In this way, we are able to study in detail how the spin precession and the spin dephasing are affected by the electric field in various conditions, such as the impurity, temperature, and spin polarization.

The in-plane electric field has two competing effects on electron spins. The most obvious one is that the electrons get a center-of-mass drift velocity and the center of the distribution functions drifts away from $\mathbf{k} = 0$. One consequence of the drift is that the DP term contributes a non-vanishing net effective magnetic field which changes the period of the spin precession. The larger the electric field is, the larger the drift velocity and consequently the net effective magnetic field is. For the electric fields we study, the net effective magnetic field is up to the order of 1 T. This moderate magnetic field has marginal effect on the SDT although it results in a distinct change in the spin precession period. Another consequence of the drift is that because more electrons are distributed at large momentum regime, the contribution of the DP term with large momentum is enhanced. Therefore the drift can reduce the SDT. In addition to the drift, the high electric field also introduces another counter effect on the spin dephasing: The scattering, which tends to drive the electrons to the steady state, is enhanced as the hot-electron effect brought by the high electric field with the electron temperature T_e higher than the background

one T . That is, the high electric field can also affect the spin dephasing through hot-electron effect. With these two effects of the electric field on spin dephasing, the electric field dependence of the spin dephasing is very rich in detail.

In small spin polarized regime, the hot-electron effect tends to enhance the SDT as the increase of the scattering rate reduces the inhomogeneous broadening. Therefore in the small electric field regime where the effect of the drift is marginal, the SDT increases with the electric field due to the hot-electron effect. For larger electric field, the effect of the drift becomes stronger. Therefore the SDT saturates under the joint actions of the drift and the hot-electron effect. When the impurity density or the background temperature T increases, the hot-electron effect reduces and the effect of the drift becomes relatively important. As a result, the increase of the SDT with the electric field is reduced. For some regimes, the SDT decreases with the increase of the electric field when the drift effect dominates.

In the high spin polarized regime where the HF term plays an important role in the spin dephasing, the hot-electron effect tends to reduce the SDT as both the increase of the electron temperature T_e and the increase of scattering reduce the HF term. Therefore, in the high spin polarization regime, the SDT decreases with the increase of the electric field.

Acknowledgments

This work was supported by the Natural Science Foundation of China under Grant No. 90303012. MWW was also supported by the “100 Person Project” of Chinese Academy of Sciences and the Natural Science Foundation of China under Grant No. 10247002. MQW was partially supported by China Postdoctoral Science Foundation.

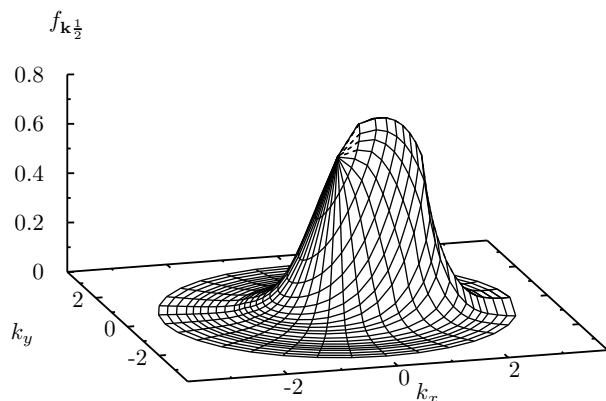


FIG. 6: A typical distribution function of spin-up electrons in the steady state with electric field $E = -0.75$ kV/cm and $P = 2.5$ %.

APPENDIX A: EFFECT OF COULOMB SCATTERING ON SPIN DEPHASING

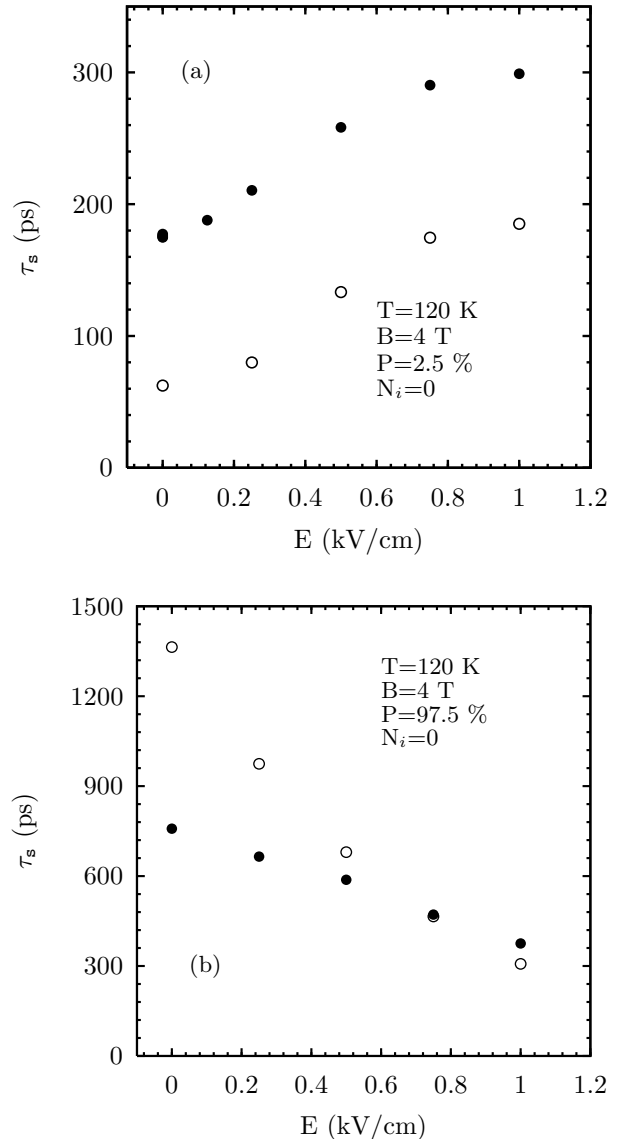


FIG. 7: Spin dephasing time in GaAs QW with (filled circle) and without (open circle) the Coulomb scattering included under different spin polarization: (a) $P=2.5$ % and (b) $P=97.5$ %.

It is stressed that the electron-electron Coulomb scattering is of particular significance in this investigation. It is not only because the Coulomb scattering is crucial in the build-up of the hot-electron temperature and the hot-electron distribution functions, but also because it has strong contribution to the spin dephasing with or without the electric field. With the Coulomb scattering, the electron distribution functions become smoother in the momentum space and electrons distribute more uniform around the drift center as shown in Fig. 6.

It is noted that the treatment of the electron-electron

scattering in the present paper takes account of the *full effect* of the Coulomb scattering which is different from our previous work^{22,23,24} where the Coulomb scattering is evaluated by replacing the distribution functions and the spin coherence in the scattering with the corresponding isotropic averages along the angle. In this way we are able to compute the electron distribution function more accurate under high electric field and to have the hot-electron effect included in our calculation. It is noted that in the absence of the applied electric field, the approximation we used before greatly reduces the CPU time and gives good qualitative results. However, this approximation is not good if one tries to get the results quantitatively.

We further show the importance of the Coulomb scattering in the spin dephasing by plotting the SDT as a function of the applied electric field with and without the Coulomb scattering in Fig. 7. As shown in the figure, for electrons with small spin polarization, the Coulomb scattering tends to drive the electrons to the equilibrium state when $E = 0$ or the steady state when applied with a finite electric field, and hence greatly reduces the inhomogeneous broadening originated from the DP term.

As a result the Coulomb scattering increases the SDT with/without applied electric fields. For the high spin polarized system, as discussed before, the effective magnetic field along the z -axis from the HF term plays an crucial role in the spin dephasing and the Coulomb scattering tends to reduce this effective magnetic field. Therefore the SDT becomes smaller when the Coulomb scattering is included.

APPENDIX B: NUMERICAL SCHEME OF THE KINETIC BLOCH EQUATIONS

In this appendix we describe the scheme of the numerical solution of the Bloch equations (3). We first rewrite the Bloch equations as following:

$$\dot{f}_{\mathbf{k},\sigma} = e\mathbf{E} \cdot \nabla_{\mathbf{k}} f_{\mathbf{k},\sigma} + \dot{f}_{\mathbf{k},\sigma}|_{\text{coh}} + \dot{f}_{\mathbf{k},\sigma}|_{\text{scatt}}, \quad (\text{B1})$$

$$\dot{\rho}_{\mathbf{k}} = e\mathbf{E} \cdot \nabla_{\mathbf{k}} \rho_{\mathbf{k}} + \dot{\rho}_{\mathbf{k}}|_{\text{coh}} + \dot{\rho}_{\mathbf{k}}|_{\text{scatt}}. \quad (\text{B2})$$

The coherent terms are

$$\left. \frac{\partial f_{\mathbf{k},\sigma}}{\partial t} \right|_{\text{coh}} = -2\sigma \{ [g\mu_B B + h_x(\mathbf{k})] \text{Im}\rho_{\mathbf{k}} + h_y(\mathbf{k}) \text{Re}\rho_{\mathbf{k}} \} + 4\sigma \text{Im} \sum_{\mathbf{q}} V_{\mathbf{q}} \rho_{\mathbf{k}+\mathbf{q}}^* \rho_{\mathbf{k}}, \quad (\text{B3})$$

$$\begin{aligned} \left. \frac{\partial \rho_{\mathbf{k}}}{\partial t} \right|_{\text{coh}} &= \frac{1}{2} [ig\mu_B B + ih_x(\mathbf{k}) + h_y(\mathbf{k})] (f_{\mathbf{k}\frac{1}{2}} - f_{\mathbf{k}-\frac{1}{2}}) \\ &+ i \sum_{\mathbf{q}} V_{\mathbf{q}} [(f_{\mathbf{k}+\mathbf{q}\frac{1}{2}} - f_{\mathbf{k}+\mathbf{q}-\frac{1}{2}}) \rho_{\mathbf{k}} - \rho_{\mathbf{k}+\mathbf{q}} (f_{\mathbf{k}\frac{1}{2}} - f_{\mathbf{k}-\frac{1}{2}})]. \end{aligned} \quad (\text{B4})$$

In these equations $V_{\mathbf{q}} = \sum_{q_z} \frac{4\pi e^2}{\kappa_0 [q^2 + q_z^2 + \kappa^2]} |I(iq_z)|^2$ with κ_0 standing for the static dielectric constant and $\kappa^2 = 6\pi N_e e^2 / (aE_f)$ denoting the screening constant. The form factor $|I(iq_z)|^2 = \pi^2 \sin^2 y / [y^2 (y^2 - \pi^2)^2]$ with $y = q_z a / 2$. The scattering terms are

$$\begin{aligned} \left. \frac{\partial f_{\mathbf{k},\sigma}}{\partial t} \right|_{\text{scatt}} &= \left\{ -2\pi \sum_{\mathbf{q}q_z\lambda} g_{\mathbf{q}\lambda}^2 \delta(\varepsilon_{\mathbf{k}} - \varepsilon_{\mathbf{k}-\mathbf{q}} - \Omega_{\mathbf{q}q_z\lambda}) [N_{\mathbf{q}q_z\lambda} (f_{\mathbf{k}\sigma} - f_{\mathbf{k}-\mathbf{q}\sigma}) + f_{\mathbf{k}\sigma} (1 - f_{\mathbf{k}-\mathbf{q}\sigma}) - \text{Re}(\rho_{\mathbf{k}} \rho_{\mathbf{k}-\mathbf{q}}^*)] \right. \\ &- 2\pi N_i \sum_{\mathbf{q}} U_{\mathbf{q}}^2 \delta(\varepsilon_{\mathbf{k}} - \varepsilon_{\mathbf{k}-\mathbf{q}}) [f_{\mathbf{k}\sigma} (1 - f_{\mathbf{k}-\mathbf{q}\sigma}) - \text{Re}(\rho_{\mathbf{k}} \rho_{\mathbf{k}-\mathbf{q}}^*)] - 2\pi \sum_{\mathbf{q}\mathbf{k}'\sigma'} V_{\mathbf{q}}^2 \delta(\varepsilon_{\mathbf{k}-\mathbf{q}} - \varepsilon_{\mathbf{k}} + \varepsilon_{\mathbf{k}'} - \varepsilon_{\mathbf{k}'-\mathbf{q}}) \\ &\left. \left[(1 - f_{\mathbf{k}-\mathbf{q}\sigma}) f_{\mathbf{k}\sigma} (1 - f_{\mathbf{k}'\sigma'}) f_{\mathbf{k}'-\mathbf{q}\sigma'} + \frac{1}{2} \rho_{\mathbf{k}} \rho_{\mathbf{k}-\mathbf{q}}^* (f_{\mathbf{k}'\sigma'} - f_{\mathbf{k}'-\mathbf{q}\sigma'}) + \frac{1}{2} \rho_{\mathbf{k}'} \rho_{\mathbf{k}'-\mathbf{q}}^* (f_{\mathbf{k}-\mathbf{q}\sigma} - f_{\mathbf{k}\sigma}) \right] \right\} \\ &- \{ \mathbf{k} \leftrightarrow \mathbf{k} - \mathbf{q}, \mathbf{k}' \leftrightarrow \mathbf{k}' - \mathbf{q} \}, \end{aligned} \quad (\text{B5})$$

$$\begin{aligned} \left. \frac{\partial \rho_{\mathbf{k}}}{\partial t} \right|_{\text{scatt}} &= \left\{ \pi \sum_{\mathbf{q}q_z\lambda} g_{\mathbf{q}\lambda}^2 \delta(\varepsilon_{\mathbf{k}} - \varepsilon_{\mathbf{k}-\mathbf{q}} - \Omega_{\mathbf{q}q_z\lambda}) [\rho_{\mathbf{k}-\mathbf{q}} (f_{\mathbf{k}\frac{1}{2}} + f_{\mathbf{k}-\frac{1}{2}}) + (f_{\mathbf{k}-\mathbf{q}\frac{1}{2}} + f_{\mathbf{k}-\mathbf{q}-\frac{1}{2}} - 2) \rho_{\mathbf{k}} - 2N_{\mathbf{q}q_z\lambda} (\rho_{\mathbf{k}} - \rho_{\mathbf{k}-\mathbf{q}})] \right. \\ &+ \pi N_i \sum_{\mathbf{q}} U_{\mathbf{q}}^2 \delta(\varepsilon_{\mathbf{k}} - \varepsilon_{\mathbf{k}-\mathbf{q}}) [(f_{\mathbf{k}\frac{1}{2}} + f_{\mathbf{k}-\frac{1}{2}}) \rho_{\mathbf{k}-\mathbf{q}} - (2 - f_{\mathbf{k}-\mathbf{q}\frac{1}{2}} - f_{\mathbf{k}-\mathbf{q}-\frac{1}{2}}) \rho_{\mathbf{k}}] \\ &\left. - \sum_{\mathbf{q}\mathbf{k}'} \pi V_{\mathbf{q}}^2 \delta(\varepsilon_{\mathbf{k}-\mathbf{q}} - \varepsilon_{\mathbf{k}} + \varepsilon_{\mathbf{k}'} - \varepsilon_{\mathbf{k}'-\mathbf{q}}) \left((f_{\mathbf{k}-\mathbf{q}\frac{1}{2}} \rho_{\mathbf{k}} + \rho_{\mathbf{k}-\mathbf{q}} f_{\mathbf{k}-\frac{1}{2}}) (f_{\mathbf{k}'\frac{1}{2}} - f_{\mathbf{k}'-\mathbf{q}\frac{1}{2}} + f_{\mathbf{k}'-\frac{1}{2}} - f_{\mathbf{k}'-\mathbf{q}-\frac{1}{2}}) \right) \right\} \end{aligned}$$

$$\begin{aligned}
& +\rho_{\mathbf{k}}\left[(1-f_{\mathbf{k}'-\frac{\mathbf{q}}{2}})f_{\mathbf{k}'-\frac{\mathbf{q}}{2}}+(1-f_{\mathbf{k}'-\frac{\mathbf{q}}{2}})f_{\mathbf{k}'-\frac{\mathbf{q}}{2}}-2\text{Re}(\rho_{\mathbf{k}'}^*\rho_{\mathbf{k}'-\mathbf{q}})\right]-\rho_{\mathbf{k}-\mathbf{q}}\left[f_{\mathbf{k}'-\frac{\mathbf{q}}{2}}(1-f_{\mathbf{k}'-\frac{\mathbf{q}}{2}})\right. \\
& \left.+(1-f_{\mathbf{k}'-\frac{\mathbf{q}}{2}})f_{\mathbf{k}'-\frac{\mathbf{q}}{2}}-2\text{Re}(\rho_{\mathbf{k}'}^*\rho_{\mathbf{k}'-\mathbf{q}})\right]\Bigg\}-\{\mathbf{k}\leftrightarrow\mathbf{k}-\mathbf{q},\mathbf{k}'\leftrightarrow\mathbf{k}'-\mathbf{q}\}, \tag{B6}
\end{aligned}$$

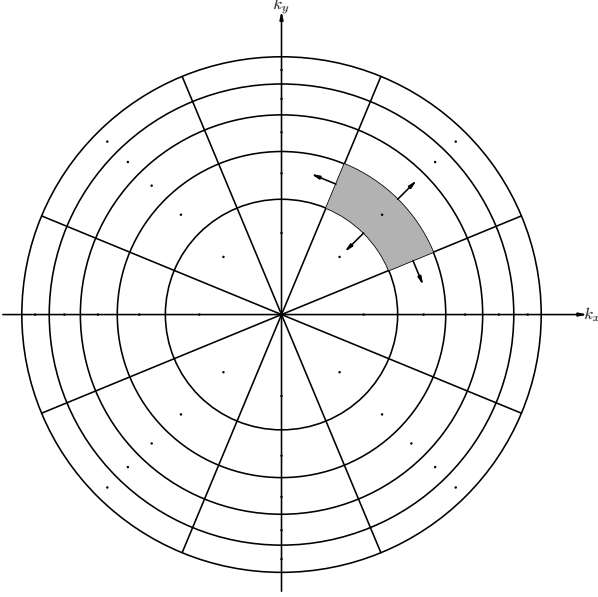


FIG. 8: The discrete momentum space.

in which $\{\mathbf{k}\leftrightarrow\mathbf{k}-\mathbf{q},\mathbf{k}'\leftrightarrow\mathbf{k}'-\mathbf{q}\}$ stands for the same terms as in the previous $\{\}$ but with the interchanges $\mathbf{k}\leftrightarrow\mathbf{k}-\mathbf{q}$ and $\mathbf{k}'\leftrightarrow\mathbf{k}'-\mathbf{q}$. In these equations $g_{\mathbf{q},q_z,\lambda}$ are the

matrix elements of electron-phonon coupling for mode λ . For LO phonons, $g_{\mathbf{q}q_z\text{LO}}^2 = \{4\pi\alpha\Omega_{\text{LO}}^{3/2}/[\sqrt{2\mu}(q^2 + q_z^2)]\}|I(iq_z)|^2$ with $\alpha = e^2\sqrt{\mu/(2\Omega_{\text{LO}})}(\kappa_\infty^{-1} - \kappa_0^{-1})$. κ_∞ is the optical dielectric constant and Ω_{LO} is the LO-phonon frequency. $N_{\mathbf{q}q_z\lambda} = 1/[\exp(\Omega_{\mathbf{q}q_z\lambda}/k_B T) - 1]$ is the Bose distribution function of phonon with mode λ at temperature T . $U_{\mathbf{q}}^2 = \sum_{q_z} \{4\pi Z_i e^2/[\kappa_0(q^2 + q_z^2)]\}^2 |I(iq_z)|^2$ is the electron-impurity interaction matrix element with Z_i standing for the charge number of the impurity. Z_i is assumed to be 1 throughout our calculation.

For numerical calculation, one first turns the Bloch equations into discrete ones. To facilitate the evaluation of the energy conservation, *i.e.* the δ -function in the scattering terms, we divide the truncated 2D momentum space into $N \times M$ control regions, each with equal energy and angle intervals as shown in Fig. 8. The \mathbf{k} -grid points are chosen to be the center of each control region and therefore are written as:

$$\mathbf{k}_{n,m} = \sqrt{2m^*E_n}(\cos\theta_m, \sin\theta_m), \tag{B7}$$

with $E_n = (n + 1/2)\Delta E$, $\theta_m = m\Delta\theta$. Here $n = 0, 1, \dots, N-1$ and $m = 0, 1, \dots, M-1$ with $E_{N-1} = E_{\text{cut}}$, the truncation energy, and $\theta_{M-1} = (M-1)2\pi/M$.

The discretization of the coherent terms is rather straightforward:

$$\left.\frac{\partial f_{\mathbf{k}_{n,m}\sigma}}{\partial t}\right|_{\text{coh}} = -2\sigma\{[g\mu_B B + h_x(\mathbf{k}_{n,m})]\text{Im}\rho_{\mathbf{k}_{n,m}} + h_y(\mathbf{k}_{n,m})\text{Re}\rho_{\mathbf{k}_{n,m}}\} + 4\sigma\text{Im}\sum_{n',m'}\Delta E\Delta\theta V_{\mathbf{k}_{n,m}-\mathbf{k}_{n',m'}}\rho_{\mathbf{k}_{n',m'}}^*\rho_{\mathbf{k}_{n,m}}, \tag{B8}$$

$$\begin{aligned} \left.\frac{\partial \rho_{\mathbf{k}_{n,m}}}{\partial t}\right|_{\text{coh}} &= \frac{1}{2}[ig\mu_B B + ih_x(\mathbf{k}_{n,m}) + h_y(\mathbf{k}_{n,m})](f_{\mathbf{k}_{n,m}\frac{1}{2}} - f_{\mathbf{k}_{n,m}-\frac{1}{2}}) \\ &+ i\sum_{n',m'}\Delta E\Delta\theta V_{\mathbf{k}_{n,m}-\mathbf{k}_{n',m'}}[(f_{\mathbf{k}_{n',m'}\frac{1}{2}} - f_{\mathbf{k}_{n',m'}-\frac{1}{2}})\rho_{\mathbf{k}_{n,m}} - \rho_{\mathbf{k}_{n',m'}}(f_{\mathbf{k}_{n,m}\frac{1}{2}} - f_{\mathbf{k}_{n,m}-\frac{1}{2}})], \end{aligned} \tag{B9}$$

For the discretization of the scattering terms, one should be more careful to ensure the energy conservation as they involve the integration of the δ -functions. If ΔE is chosen to satisfy $\Omega_0 = n_{\text{LO}}\Delta E$ with n_{LO} being an integer, the integration of the δ -function in the electron-LO phonon scattering term can be carried out. After carrying out the integration of the δ -functions, the electron-LO phonon and electron-impurity scattering terms read

$$\begin{aligned} \dot{f}_{\mathbf{k}_{n,m}\sigma}\Big|_{\text{scatt}}^{\text{imp+LO}} &= -\frac{m^*}{2\pi}\sum_{m'q_z}\Delta\theta g_{\mathbf{k}_{n,m}-\mathbf{k}_{n-n_{\text{LO}},m'},q_z,\text{LO}}^2\theta(n-n_{\text{LO}})[N_{0\text{LO}}(f_{\mathbf{k}_{n,m}\sigma} - f_{\mathbf{k}_{n-n_{\text{LO}},m'}\sigma}) + f_{\mathbf{k}_{n,m}\sigma}(1 - f_{\mathbf{k}_{n-n_{\text{LO}},m'}\sigma}) \\ &- \text{Re}(\rho_{\mathbf{k}_{n,m}}\rho_{\mathbf{k}_{n-n_{\text{LO}},m'}}^*)] + \frac{m^*}{2\pi}\sum_{m'q_z}\Delta\theta g_{\mathbf{k}_{n,m}-\mathbf{k}_{n+n_{\text{LO}},m'},q_z,\text{LO}}^2\theta(N-n-n_{\text{LO}})[N_{0\text{LO}}(f_{\mathbf{k}_{n+n_{\text{LO}},m'}\sigma} - f_{\mathbf{k}_{n,m}\sigma}) \\ &+ f_{\mathbf{k}_{n+n_{\text{LO}},m'}\sigma}(1 - f_{\mathbf{k}_{n,m}\sigma}) - \text{Re}(\rho_{\mathbf{k}_{n+n_{\text{LO}},m'}}\rho_{\mathbf{k}_{n,m}}^*)] - \frac{m^*}{2\pi}N_i\sum_m\Delta\theta U_{\mathbf{k}_{n,m}-\mathbf{k}_{n,m'}}^2(f_{\mathbf{k}_{n,m}} - f_{\mathbf{k}_{n,m'}}) \end{aligned} \tag{B10}$$

The electron-electron Coulomb scattering is more complicated after the integration of the δ -function:

$$\begin{aligned} \dot{f}_{n,m\sigma} \Big|_{\text{scatt}}^{\text{Coul}} &= -\frac{m^{*2}}{(2\pi)^2} \sum_{n_1, m_1, n_2, \sigma'} \Delta E \Delta \theta \frac{\sqrt{4E'E_{n_2+1} - (E_n - E_{n_1} + E')^2} - \sqrt{4E'E_{n_2} - (E_n - E_{n_1} + E')^2}}{2E'} V_{\mathbf{k}_{n,m} - \mathbf{k}_{n_1, m_1}}^2 \\ &\times \left[(1 - f_{\mathbf{k}_{n_1, m_1} \sigma}) f_{\mathbf{k}_{n,m} \sigma} (1 - f_{\mathbf{k}_{n_2, m_2'} \sigma'}) f_{\mathbf{k}_{n_3, m_3'} \sigma'} - (1 - f_{\mathbf{k}_{n,m} \sigma}) f_{\mathbf{k}_{n_1, m_1} \sigma} (1 - f_{\mathbf{k}_{n_3, m_3'} \sigma'}) f_{\mathbf{k}_{n_2, m_2'} \sigma'} \right. \\ &\left. + \rho_{\mathbf{k}_{n,m}} \rho_{\mathbf{k}_{n_1, m_1}}^* (f_{\mathbf{k}_{n_2, m_2'} \sigma'} - f_{\mathbf{k}_{n_3, m_3'} \sigma'}) + \rho_{\mathbf{k}_{n_2, m_2'}} \rho_{\mathbf{k}_{n_3, m_3'}}^* (f_{\mathbf{k}_{n_1, m_1} \sigma} - f_{\mathbf{k}_{n,m} \sigma}) \right]. \end{aligned} \quad (\text{B11})$$

Here $n_3 = n - n_1 + n_2$. m_2' and m_3' are defined as

$$m_2' \Delta \theta = \theta_2 + \theta_{\mathbf{k}_{n,m}, \mathbf{k}_{n_1, m_1}}, \quad (\text{B12})$$

$$m_3' \Delta \theta = \theta_1 + \theta_{\mathbf{k}_{n,m}, \mathbf{k}_{n_1, m_1}}, \quad (\text{B13})$$

in which $\theta_{\mathbf{k}_{n,m}, \mathbf{k}_{n_1, m_1}}$ standing for the angle between the wave vectors $\mathbf{k}_{n,m}$ and \mathbf{k}_{n_1, m_1} . θ_1 and θ_2 are defined as

$$\cos \theta_1 = \frac{E_{n_1} - E_n + E'}{2\sqrt{E_{n_3} E'}}, \quad (\text{B14})$$

$$\cos \theta_2 = -\frac{E_n - E_{n_1} + E'}{2\sqrt{E_{n_2} E'}}, \quad (\text{B15})$$

with $E' = (\mathbf{k}_{n,m} - \mathbf{k}_{n_1, m_1})^2 / 2m^*$. Unfortunately, m_2' and m_3' here are not integers and therefore the values of $f_{\mathbf{k}_{n_2, m_2'} \sigma}$, $\rho_{\mathbf{k}_{n_2, m_2'}}$, $f_{\mathbf{k}_{n_3, m_3'} \sigma}$ and $\rho_{\mathbf{k}_{n_3, m_3'}}$ are unknown. In our computation, we approximate them to be the interpolation of the nearest grid points with the same energy.

The driving terms should be treated with caution as the equations are stable only for some finite differential schemes, such as forward differencing and central differencing schemes. In this study, we use the forward differencing scheme. However, the usual expression of this scheme is based on the Taylor series expansion and is difficult to apply to the polar coordinate system which we use in this work. This difficulty can be circumvented by the so called discrete conservation principle:⁵⁵

$$e\mathbf{E} \cdot \nabla_{\mathbf{k}} f_{\mathbf{k}, \sigma} \Big|_{\mathbf{k}=\mathbf{k}_{n,m}} \simeq \frac{\int_{\Omega_{n,m}} d^2k e\mathbf{E} \cdot \nabla_{\mathbf{k}} f_{\mathbf{k}, \sigma}}{m^* \Delta E \Delta \theta}$$

$$\begin{aligned} &= \frac{1}{m^* \Delta E \Delta \theta} \int_{\partial\Omega_{n,m}} ds e\mathbf{E} \cdot \hat{\mathbf{n}} f_{\mathbf{k}, \sigma} \\ &= \frac{1}{m^* \Delta E \Delta \theta} \sum_{n'm'} \int_{\Omega_{n,m} \cap \Omega_{n', m'}} ds e\mathbf{E} \cdot \hat{\mathbf{n}} f_{\mathbf{k}, \sigma} \\ &\simeq \frac{1}{m^* \Delta E \Delta \theta} \sum_{n'm'} e\mathbf{E} \cdot \hat{\mathbf{n}}_{n,m}^{n'm'} s_{n,m}^{n'm'} f_{\mathbf{k}_{n,m}, \sigma}. \end{aligned} \quad (\text{B16})$$

Here $\Omega_{n,m}$ and $\partial\Omega_{n,m}$ are the control region which contains the grid point $\mathbf{k}_{n,m}$ and the corresponding boundary. In the last step of the above equation, the integration of the boundary is replaced by the summation over the first order quadrature on the four (or three if the control region is the neighbor of $\mathbf{k} = 0$) sides of the boundary $\partial\Omega_{n,m}$ with $s_{n,m}^{n'm'}$ and $\hat{\mathbf{n}}_{n,m}^{n'm'}$ standing for the length and the outward normal to the boundary $\Omega_{nm} \cap \Omega_{n'm'}$. In order to satisfy the request of the numerical stability, $\mathbf{k}_{n,m}'$ is chosen to be $\mathbf{k}_{n,m}$ if $-e\mathbf{E} \cdot \hat{\mathbf{n}}_{nm}^{n'm'} > 0$ and $\mathbf{k}_{n', m}'$ otherwise.

It is noted that this choice of \mathbf{k} makes our approach identify to the forward differencing scheme. The time evolution is computed by the fourth-order Runge-Kutta method.⁵⁶ The computation is carried out in a parallel manner in the ‘‘Beowulf’’ cluster. For a typical calculation, it takes about 7.5 hours to get one SDT with 16-node AMD Athlon XP2800+ CPU’s when both N and M are chosen to be 32.

* Author to whom correspondence should be addressed; Electronic address: mwwu@ustc.edu.cn

† Mailing Address

¹ S. A. Wolf, *J. Supercond.: Incorporing Novel Mechanism* **13**, 195 (2000).

² M. Ziese and M. J. Thornton, eds., *Spin Electronics* (Springer, Berlin, 2001).

³ E. M. Conwell, *Solid State Physics*, vol. suppl. 9 (Academic Press, New York, 1967).

⁴ E. M. Conwell, *High field transport in semiconductors* (Pergamon, Oxford, 1972).

⁵ J. M. Kikkawa, I. P. Smorchkova, N. Samarth, and D. D. Awschalom, *Science* **277**, 1284 (1997).

⁶ J. M. Kikkawa and D. D. Awschalom, *Nature* **397**, 139 (1998).

⁷ J. M. Kikkawa and D. D. Awschalom, *Phys. Rev. Lett.* **80**, 4313 (1998).

⁸ H. Ohno, *Science* **281**, 951 (1998).

⁹ Y. Ohno, R. Terauchi, T. Adachi, F. Matsukura, and H. Ohno, *Phys. Rev. Lett.* **83**, 4196 (1999).

¹⁰ R. I. Dzhioev, B. P. Zakharchenya, V. L. Korenev, D. Gammon, and D. S. Katzer, *JETP Lett.* **74**, 182 (2001).

¹¹ R. I. Dzhioev, K. V. Kavokin, V. L. Korenev, M. V. Lazarev, B. Y. Meltser, M. N. Stepanova, B. P. Zakharchenya, D. Gammon, and D. S. Katzer, *Phys. Rev. B* **66**, 245204 (2002).

- ¹² F. Meier and B. P. Zakharchenya, eds., *Optical Orientation* (North-Holland, Amsterdam, 1984).
- ¹³ Y. Yafet, Phys. Rev. **85**, 478 (1952).
- ¹⁴ R. J. Elliot, Phys. Rev. **96**, 266 (1954).
- ¹⁵ G. L. Bir, A. G. Aronov, and G. E. Pikus, Zh. Eksp. Teor. Fiz. **69**, 1382 (1975), [Sov. Phys.-JETP **42**, 705 (1975)].
- ¹⁶ M. I. D'yakonov and V. I. Perel', Zh. Eksp. Teor. Fiz. **60**, 1954 (1971), [Sov. Phys.-JETP **33**, 1053 (1971)].
- ¹⁷ M. W. Wu and C. Z. Ning, Eur. Phys. J. B. **18**, 373 (2000).
- ¹⁸ M. W. Wu, J. Supercond.: Incorporating Novel Mechanism **14**, 245 (2001), cond-mat/0109258.
- ¹⁹ M. W. Wu and C. Z. Ning, phys. stat. sol. (b) **222**, 523 (2000).
- ²⁰ M. W. Wu, J. Phys. Soc. Jpn. **70**, 2195 (2001).
- ²¹ M. W. Wu and M. Kuwata-Gonokami, Solid State Commun. **121**, 509 (2002).
- ²² M. Q. Weng and M. W. Wu, Phys. Rev. B **68**, 075312 (2003).
- ²³ M. Q. Weng and M. W. Wu, J. Phys.:Condens. Matter **15**, 5563 (2003).
- ²⁴ M. Q. Weng and M. W. Wu, Phys. Stat. Sol. (b) **239**, 121 (2003).
- ²⁵ J. L. Cheng, M. Q. Weng, and M. W. Wu, Solid State Commun. **128**, 365 (2003).
- ²⁶ D. Hägele, M. Oestreich, W. W. Rühle, N. Nestle, and K. Eberl, Appl. Phys. Lett. **73**, 1580 (1998).
- ²⁷ H. Sanada, I. Arata, Y. Ohno, Z. Chen, K. Kayanuma, Y. Oka, F. Matsukura, and H. Ohno, Appl. Phys. Lett. **81**, 2788 (2002).
- ²⁸ I. Malajovich, J. J. Berry, N. Samarth, and D. D. Awschalom, Nature **411**, 770 (2001).
- ²⁹ G. Schmidt et al., Phys. Rev. B **62**, R4790 (2000).
- ³⁰ Y. Qi and S. Zhang, Phys. Rev. B **67**, 052407 (2003).
- ³¹ A. Bournel, P. Dollfus, P. Bruno, and P. Hesto, ULTRA-FAST PHENOMENA IN SEMICONDUCTORS MATERIALS SCIENCE FORUM **297**, 205 (1999).
- ³² A. Bournel, P. Dollfus, P. Bruno, and P. Hesto, Physica B **272**, 331 (1999).
- ³³ A. Bournel, P. Dollfus, P. Bruno, and P. Hesto, Solid State Communications **104**, 85 (1997).
- ³⁴ S. Saikin, M. Shen, M.-C. Cheng, and V. Privman, J. Appl. Phys. **94**, 1769 (2003).
- ³⁵ M. Shen, S. Saikin, M.-C. Cheng, and V. Privman, cond-mat/0309118.
- ³⁶ S. Pramanik, S. Bandyopadhyay, and M. Cahay, Phys. Rev. B **68**, 075313 (2003).
- ³⁷ S. Pramanik, S. Bandyopadhyay, and M. Cahay, cond-mat/0310245.
- ³⁸ Y. A. Bychkov and E. I. Rashba, J. Phys. C **17**, 6039 (1984).
- ³⁹ Y. A. Bychkov and E. I. Rashba, JETP Lett. **39**, 78 (1984).
- ⁴⁰ E. I. Rashba and A. L. Efros, cond-mat/0310192.
- ⁴¹ M. W. Wu and H. Metiu, Phys. Rev. B **61**, 2945 (2000).
- ⁴² M. Q. Weng and M. W. Wu, Phys. Rev. B **66**, 235109 (2002).
- ⁴³ M. Q. Weng and M. W. Wu, J. Appl. Phys. **93**, 410 (2003).
- ⁴⁴ M. Q. Weng, M. W. Wu, and Q. W. Shi, Phys. Rev. B **69** (2004), in Press.
- ⁴⁵ A. P. Dmitriev, V. Y. Kachorovskii, M. S. Shur, and M. Strocio, solid state comm. **113**, 565 (2000).
- ⁴⁶ A. P. Dmitriev, V. Y. Kachorovskii, and M. S. Shur, J. Appl. Phys. **89**, 3793 (2001).
- ⁴⁷ G. Dresselhaus, Phys. Rev. **100**, 580 (1955).
- ⁴⁸ A. G. Aronov, G. E. Pikus, and A. N. Titkov, Zh. Eksp. Teor. Fiz. **84**, 1170 (1983), [Sov. Phys.-JETP **57**, 680 (1983)].
- ⁴⁹ G. D. Mahan, *Many-particle Physics* (Plenum, New York, 1981).
- ⁵⁰ H. Haug and A. P. Jauho, *Quantum Kinetics in Transport and Optics of Semiconductors* (Springer-Verlag, Berlin, 1996).
- ⁵¹ T. Kuhn and F. Rossi, Phys. Rev. Lett. **69**, 977 (1992).
- ⁵² M. A. Brand, A. Malinowski, O. Z. Karimov, P. A. Marsden, R. T. Harley, A. J. Shields, D. Sanvitto, D. A. Ritchie, and M. Y. Simmons, Phys. Rev. Lett. p. 236601 (2002).
- ⁵³ X. L. Lei and C. S. Ting, Phys. Rev. B **30**, 4809 (1984).
- ⁵⁴ A. Malinowski, R. S. Britton, T. Grevatt, R. T. Harley, D. A. Ritchie, and M. Y. Simmons, Phys. Rev. B **62**, 13034 (2000).
- ⁵⁵ V. Meiser, ed., *Computational Science Education Project* (1993), electronic book, available from <http://csep1.phy.ornl.gov/csep.html>.
- ⁵⁶ W. H. Press, S. A. Teukolsky, and W. T. Vetterling, *Numerical Recipes in Fortran 77: The Art of Scientific Computing* (Cambridge University Press, Cambridge, 1988).